

# Spin loop-current textures in the Hubbard models

Kazuya Shinjo,<sup>1</sup> Shigetoshi Sota,<sup>2,3</sup> Seiji Yunoki,<sup>1,2,3,4</sup> and Takami Tohyama<sup>5</sup>

<sup>1</sup>*Computational Quantum Matter Research Team,*

*RIKEN Center for Emergent Matter Science (CEMS), Wako, Saitama 351-0198, Japan*

<sup>2</sup>*Computational Materials Science Research Team,*

*RIKEN Center for Computational Science (R-CCS), Kobe, Hyogo 650-0047, Japan*

<sup>3</sup>*Quantum Computational Science Research Team,*

*RIKEN Center for Quantum Computing (RQC), Wako, Saitama 351-0198, Japan*

<sup>4</sup>*Computational Condensed Matter Physics Laboratory,*

*RIKEN Cluster for Pioneering Research (CPR), Saitama 351-0198, Japan*

<sup>5</sup>*Department of Applied Physics, Tokyo University of Science, Tokyo 125-8585, Japan*

(Dated: May 24, 2023)

The recent experimental observations of loop current in  $\text{Sr}_2\text{IrO}_4$ ,  $\text{YBa}_2\text{Cu}_3\text{O}_7$ , and  $\text{Sr}_{14}\text{Cu}_{24}\text{O}_{41}$  have inspired a theoretical study that broadly redefines loop current as a manifestation of quantum liquid crystals. Using the density-matrix renormalization group method, here we investigate the emergence of spin loop-current (sLC) textures in carrier-doped (i) excitonic insulators, (ii) orbital-selective Mott insulators, and (iii) two-dimensional Mott insulators, modeled by a two-orbital Hubbard model on a ladder lattice in (i) and (ii) and a single-orbital Hubbard model on a square lattice in (iii). Calculating the spatial distribution of spin current around a bond to which a pinning field is applied, we find conditions for longer-ranged sLC correlations. In system (i), using typical sets of model parameters for  $\text{Pr}_{0.5}\text{Ca}_{0.5}\text{CoO}_3$ , we find that a sLC texture appears near half filling, associated with an excitonic condensation in a spin channel. In system (ii), using typical sets of model parameters for  $\text{BaFe}_2\text{Se}_3$ , we find that a sLC texture appears at electron fillings where a block-type antiferromagnetism develops. In system (iii), introducing a next-nearest-neighbor hopping  $t' \sim -0.25$  (in unit of the nearest neighbor hopping) suggested for high- $T_c$  cuprates, we find that an axial-sLC texture emerges at hole-carrier density  $\delta = 0.125$ , where the charge stripe simultaneously appears.

## I. INTRODUCTION

Unexpected phenomena often emerge in quantum many-body systems and are most pronounced when strong quantum fluctuations are present in strongly correlated electron systems. According to Landau, many-body phases of matter exhibit spontaneous symmetry breaking at low temperatures, and phase transitions are characterized by symmetry changes. However, for example, quantum spin liquids do not break any symmetry and hence are not characterized by any local order parameter, indicating the presence of quantum phases beyond the description of the Landau's symmetry-breaking theory. Furthermore, an intermediate state between spontaneous symmetry-broken and symmetry-unbroken states has been proposed as a quantum liquid crystal [1–6]. Namely, a quantum liquid crystal is regarded as a quantum state with partially broken spatial symmetry and can exhibit unconventional properties since the partially symmetry-breaking order can interplay with other intrinsic orders such as superconducting and magnetic orders.

A quantum nematic state [7–12] is one of the most well-known examples of quantum liquid crystals, but there is another quantum liquid crystal with spontaneous loop current. Although quantum states with loop current, also called staggered-flux or orbital-antiferromagnetic states, have a long history in the field of strongly correlated electron systems [13–17], they have attracted renewed interest in the last decade. This is due to the recent

discovery of a series of quantum states with various charge loop-current (cLC) textures in  $\text{Sr}_2\text{IrO}_4$  [18, 19],  $\text{YBa}_2\text{Cu}_3\text{O}_7$  [20, 21], and  $\text{Sr}_{14}\text{Cu}_{24}\text{O}_{41}$  [22] via the improved measurements of the Kerr effect, polarized neutron scattering, magnetic torque, and second-harmonic generation. Theoretically, cLC textures have been extensively studied based on the Hubbard models [23–27] as a cLC long-range order [28–30] or its fluctuation [31] was suggested to characterize the pseudogap phase in high- $T_c$  cuprate superconductors. However, no numerical evidence of cLC textures has been reported in single- and three-orbital Hubbard models [23–27]. It has been proposed that quantum states with cLC textures can be present in a generalized Hubbard ladder [32–35] and spinless Hubbard model [36–38] if unrealistic interactions for real materials are introduced.

The recent observations described above have encouraged further theoretical investigation of loop-current textures from a different point of view. One such viewpoint is to explore the possibility of quantum states with spin current rather than charge current [39, 40]. Due to the difficulty of treating strongly correlated electron systems, many theoretical studies rely on the mean-field or perturbation theory. Here, instead, we address the question of whether non-perturbative treatment can elucidate quantum states with spin loop-current (sLC) textures in the Hubbard models.

For this purpose, we employ the density-matrix renormalization group (DMRG) method to investigate the possibility of quantum states with sLC in the Hubbard

models. In particular, we consider three kinds of strongly correlated electron systems in this paper: carrier-doped (i) excitonic insulators, (ii) orbital-selective Mott insulators, and (iii) two-dimensional Mott insulators, modeled by a two-orbital Hubbard ladder with a crystal field for (i) and (ii) and a single-orbital Hubbard model on a square lattice for (iii). In the two-orbital model, we introduce the Hund coupling and pair hopping in addition to the Coulomb interaction. Calculating the spatial distribution of spin current around a bond to which a pinning field is applied, we examine whether there are cases where sLC correlations can be enhanced.

We find that such cases exist, i.e., sLC textures emerging for each of these systems (i)–(iii). In system (i), the correlations of sLCs are enhanced, if we introduce an inter-orbital hopping in the model. This is consistent with a previous study of dynamical mean-field theory [39]. The emergence of sLC textures is associated with exciton condensation in a spin channel, which is suggested to be realized in  $\text{Pr}_{0.5}\text{Ca}_{0.5}\text{CoO}_3$  [41]. System (ii) is known to exhibit a stripe- and block-type antiferromagnetic (AFM) phases [42], which have been observed experimentally in  $\text{BaFe}_2\text{X}_3$  ( $X = \text{Se}, \text{S}$ ) [43–45]. We find a quantum state with sLC textures in the vicinity of the block-type AFM phase. In contrast to system (i), the inter-orbital hopping is not relevant to generating sLC textures here. The carrier density where the correlations of sLC are significantly enhanced corresponds to that in a generalized Kondo-Heisenberg model (GKHM) where vector chirality order appears [46]. In system (iii), we find that the correlations of sLCs are enhanced when we introduce an appropriate value of the next-nearest-neighbor hopping  $t'$ . The sLC textures found here emerge at hole density  $\delta = 0.125$  and coexist with charge stripes.

Our findings clearly show that sLC textures can spontaneously emerge by introducing carriers and/or orbital degrees of freedom to increase quantum fluctuations, which induce quantum liquid crystalinity. Therefore, our approach, which does not rely on the mean-field or perturbation theory, will bring a new perspective to the study of quantum liquid crystals.

The rest of this paper is organized as follows. We first introduce the phenomenological theory of quantum liquid crystal with sLC textures in Sec. II. We then show the results of our DMRG study of two-orbital Hubbard ladders in Sec. III. In Sec. III A, we numerically demonstrate that sLC textures emerge in a carrier-doped excitonic insulator. Here, the inter-orbital hopping and crystal field are necessary for inducing excitonic condensation with sLC textures. In Sec. III B, we show that sLC textures arise in a carrier-doped orbital-selective Mott insulator, where the introduction of an appropriate carrier density and the different degree of localization in the two orbitals are both necessary to achieve sLC textures. Next, we show in Sec. IV the results on a single-orbital Hubbard model on a square lattice, for which the intermediate value of  $t'$  is necessary for sLC textures that emerge at hole density  $\delta = 0.125$ . Finally, we summarize this paper in Sec. V.

## II. QUANTUM LIQUID CRYSTAL WITH SPIN LOOP-CURRENT TEXTURES

Quantum liquid crystals in two dimensions have been discussed on the basis of the Pomeranchuk instability [47] in the Landau's Fermi liquid theory [48, 49]. The Landau Hamiltonian [5, 9, 50] of interacting electrons described by the field operator  $\Psi_\tau(\mathbf{r})$  ( $\tau = \uparrow, \downarrow$ : spin,  $\mathbf{r}$ : real-space position) in two dimensions is written as

$$\mathcal{H}_L = \sum_{\tau} \int d^2\mathbf{r} \Psi_{\tau}^{\dagger}(\mathbf{r}) \varepsilon(\nabla) \Psi_{\tau}(\mathbf{r}) + \frac{1}{2} \sum_{l,p} \int d^2\mathbf{r} d^2\mathbf{r}' f_l^p(\mathbf{r} - \mathbf{r}') Q_l^p(\mathbf{r}) Q_l^p(\mathbf{r}'), \quad (1)$$

where  $\varepsilon(\nabla)$  is single-particle energy,  $Q_l^p(\mathbf{r})$  is a  $l$ -th order complex order parameter in a charge ( $p = c$ ) or spin ( $p = a$ ) channel, and  $f_l^p(\mathbf{r} - \mathbf{r}')$  is an interaction function. The order parameters for quantum liquid crystals are given as

$$\langle Q_l^c(\mathbf{r}) \rangle = \sum_{\tau} \langle \Psi_{\tau}^{\dagger}(\mathbf{r}) (\partial_x + i\partial_y)^l \Psi_{\tau}(\mathbf{r}) \rangle \quad (2)$$

and

$$\langle Q_l^a(\mathbf{r}) \rangle = \sum_{\tau, \tau'} \langle \Psi_{\tau}^{\dagger}(\mathbf{r}) \sigma_{\tau\tau'}^a (\partial_x + i\partial_y)^l \Psi_{\tau'}(\mathbf{r}) \rangle \quad (3)$$

for particle-hole pair condensations with orbital angular momentum  $l$  in a charge channel [9] and a spin channel [50, 51], respectively. Here,  $\sigma_{\tau\tau'}^a$  in Eq. (3) indicates a matrix element of the Pauli matrix  $\sigma^a$  with  $a = x, y$ , and  $z$ .

A quantum liquid crystal with nonzero  $\langle Q_l^p \rangle$  may be induced by the Pomeranchuk instability of the Fermi surfaces [47]. Taking the density of states at the Fermi energy  $N_F$ , the Landau parameters  $F_l^p = N_F f_l^p(\mathbf{q} = \mathbf{0})$  where  $f_l^p(\mathbf{q}) = \int d\mathbf{r} e^{i\mathbf{q}\cdot\mathbf{r}} f_l^p(\mathbf{r})$  quantifies the strength of the forward scattering interactions among quasiparticles at low energies close to the Fermi surface in a charge or spin channel. The thermodynamic stability of the Fermi liquid state requires that the Landau parameters  $F_l^p$  cannot be too negative. Namely, the thermodynamic instability occurs when  $F_l^p < -(2l + 1)$ . The most typical Pomeranchuk instabilities are found in the  $s$ -wave channel: the Stoner ferromagnetism with  $\langle Q_0^a \rangle \neq 0$  and the phase separation with  $\langle Q_0^c \rangle \neq 0$  are induced at  $F_0^a < -1$  and  $F_0^c < -1$ , respectively. For higher  $l$ , the Pomeranchuk instabilities in charge channel  $F_2^c$  and  $F_3^c$  induce a spontaneous symmetry breaking, leading to a charge nematic state and a quantum state with cLC textures, respectively. Another kind of quantum liquid crystal is realized in spin channels  $F_l^a$  with  $l > 0$  [50, 51], which breaks spin-orbital symmetry as originally proposed in  $^3\text{He}$  [49, 52]. An emergent Rashba [53]-Dresselhaus [54]-like spin-orbit coupling can lead to a quantum state with sLC textures [50, 51, 55]. In the following sections, we show the results of our microscopic study of quantum states with sLC textures.

### III. TWO-ORBITAL HUBBARD LADDERS

#### A. Carrier-doped excitonic insulators

The order parameter  $\langle Q^p \rangle$  of a quantum liquid crystal is particle-hole pair condensation, which is analogous to exciton condensation in semimetals [13, 56–59]. The emergence of sLC textures associated with exciton condensation has been suggested previously in the (dynamical) mean-field analysis [39, 60, 61]. The sLC textures are associated with exciton condensation in the spin channel, which is stabilized in the presence of the Hund’s coupling and pair hopping [62]. Furthermore, the pair field of exciton condensation can be imaginary when an inter-orbital hopping is suitably selected [39, 63].

Here, we numerically investigate sLC textures associated with exciton condensation in the spin channel. Our study is based on the two-orbital Hubbard model on a ladder lattice. In the SU(2)-symmetric form, it is given by the following Hamiltonian:

$$\begin{aligned} \mathcal{H}_{\text{TH}} = & - \sum_{\langle i,j \rangle, \gamma, \gamma', \tau} t_{\gamma\gamma'} (c_{i,\gamma,\tau}^\dagger c_{j,\gamma',\tau} + \text{H.c.}) \\ & + U \sum_{i,\gamma} n_{i,\gamma,\uparrow} n_{i,\gamma,\downarrow} + (U - 5J_{\text{H}}/2) \sum_i n_{i,a} n_{i,b} \\ & - 2J_{\text{H}} \sum_i \mathbf{S}_{i,a} \cdot \mathbf{S}_{i,b} + J_{\text{H}} \sum_i (P_{i,a}^\dagger P_{i,b} + \text{H.c.}), \end{aligned} \quad (4)$$

where  $c_{i,\gamma,\tau}^\dagger$  is the electron creation operator at site  $i$  with spin  $\tau = \uparrow, \downarrow$  and orbital  $\gamma = a, b$ .  $n_{i,\gamma} = \sum_\tau n_{i,\gamma,\tau}$  is the total charge density operator for orbital  $\gamma$  at site  $i$ , where  $n_{i,\gamma,\tau} = c_{i,\gamma,\tau}^\dagger c_{i,\gamma,\tau}$ .

The first term of the Hamiltonian  $\mathcal{H}_{\text{TH}}$  represents the nearest-neighbor electron hopping from orbital  $\gamma$  at site  $i$  to orbital  $\gamma'$  at site  $j$  and vice versa with a hopping amplitude  $t_{\gamma\gamma'}$ .  $\langle i, j \rangle$  is a nearest-neighbor pair of sites at  $i$  and  $j$ . The second term represents the intra-orbital Coulomb interaction with its magnitude  $U$ . The third term represents the inter-orbital Coulomb interaction. The fourth term represents the Hund’s coupling  $J_{\text{H}}$  between spins  $\mathbf{S}_{i,\gamma} = (S_{i,\gamma}^x, S_{i,\gamma}^y, S_{i,\gamma}^z)$  at different orbitals with  $S_{i,\gamma}^a = \frac{1}{2} \sum_{\tau, \tau'} c_{i,\gamma,\tau}^\dagger \sigma_{\tau,\tau'}^a c_{i,\gamma,\tau'}$ . The last term represents the on-site inter-orbital pair hopping with  $P_{i,\gamma} = c_{i,\gamma,\uparrow} c_{i,\gamma,\downarrow}$ .

In addition, we extend this Hamiltonian by introducing the following crystal-field splitting term

$$\mathcal{H}_{\text{CF}} = \frac{\Delta}{2} \sum_{i,\tau} (n_{i,a,\tau} - n_{i,b,\tau}). \quad (5)$$

Therefore, the total Hamiltonian  $\mathcal{H}_{\text{ETH}}$  of an extended two-orbital Hubbard model (ETHM) is described by  $\mathcal{H}_{\text{ETH}} = \mathcal{H}_{\text{TH}} + \mathcal{H}_{\text{CF}}$ . Following Refs. [39, 41], we set the model parameters as  $U = 4$ ,  $J_{\text{H}} = U/4$ , and  $(t_{aa}, t_{bb}) = (0.4, -0.2)$  in the unit of eV, which are used to capture the basic features of perovskite cobaltites. Note

that we introduce the on-site inter-orbital pair hopping term, which is ignored in Refs. [39, 60, 61, 63]. At half filling, a band (Mott) insulator is stable for large (small)  $\Delta$ , while an excitonic insulator can be realized for intermediate  $\Delta$ .

The continuity equation along with the Heisenberg equation of motion for a spin operator  $S_{i,\gamma}^z$  leads to a spin-current operator

$$j_{\gamma\gamma'}^s(\mathbf{r}_{lm}) := i (\text{sgn } t_{\gamma\gamma'}) \sum_\tau \frac{s_\tau}{2} \left( c_{l,\gamma,\tau}^\dagger c_{m,\gamma',\tau} - c_{m,\gamma',\tau}^\dagger c_{l,\gamma,\tau} \right) \quad (6)$$

for a bond  $(l, m)$  connecting sites  $l$  and  $m$  denoted as  $\mathbf{r}_{lm}$ , where  $s_\tau = +1 (-1)$  for  $\tau = \uparrow (\downarrow)$ . To investigate the spin current, we use a pinning-field approach [32, 33, 35, 64–66], where we introduce a small pinning field  $j_{\gamma\gamma'}^s(\mathbf{r}_{lm})$  on a bond  $(l, m)$  of orbital  $\gamma$  and  $\gamma'$  described by  $\mathcal{H}_{\gamma\gamma'}^s = -h |t_{\gamma\gamma'}| j_{\gamma\gamma'}^s(\mathbf{r}_{lm})$  with  $h = 0.0001$ . Note that conclusions obtained from this approach are essentially the same as those obtained from correlation functions [33, 35]. The pinning-field approach has an advantage because the DMRG method can calculate local quantities with much better accuracy than correlation functions [64, 66]. Although the computational cost increases because complex numbers have to be used, the pinning field approach has been applied successfully for the DMRG study of off-diagonal orders or fluctuations of superconducting pairs and current, which are usually difficult to detect.

Figure 1 shows the results of  $\langle j_{\gamma\gamma'}^s(\mathbf{r}_{lm}) \rangle$  for three different values of  $\Delta = 2.6, 3$ , and  $3.4$ , when the inter-orbital hoppings  $t_{ab} = t_{ba} = 0.05$  are introduced. Note that this type of the inter-orbital hoppings satisfying  $t_{ab}t_{ba} > 0$  is usually referred to as “even”. These results are obtained near half filling, i.e., electron density  $n = N/L = 1.92$ , where  $N$  is the total number of electrons and  $L = L_x L_y$  is the number of sites. Note that  $n = 2$  corresponds to half filling in the ETHM. We evaluate the ground state for the two-leg ladder with  $(L_x, L_y) = (24, 2)$ , keeping  $\chi = 2500$  largest density-matrix eigenstates and taking 40 sweeps, which leads to a truncation error less than  $10^{-11}$ . The pinning field is introduced in the bond of orbital  $b$  that is indicated by an arrow with “pinning” in Fig. 1. Even when the pinning field is applied to orbital  $a$ , the following argument remains qualitatively the same. Since the expectation values of the spin current increase in proportion to the density of states at the Fermi level, we normalize these quantities by  $|\langle j_{\gamma\gamma'}^s(\mathbf{r}_{lm}) \rangle|$  at the bond applied with the pinning field in order to compare the results among different electronic states.

We find in Fig. 1(b) that the signal of sLC is most enhanced with clear sLC textures for  $\Delta = 3$ , where exciton condensation in the spin channel is associated [67]. For larger and smaller values of  $\Delta$ , i.e.,  $\Delta = 2.6$  and  $\Delta = 3.4$ , where excitons are not condensed, no sLC textures are observed in Figs. 1(a) and 1(c). Note that the presence of Hund’s coupling is crucial for realizing exciton

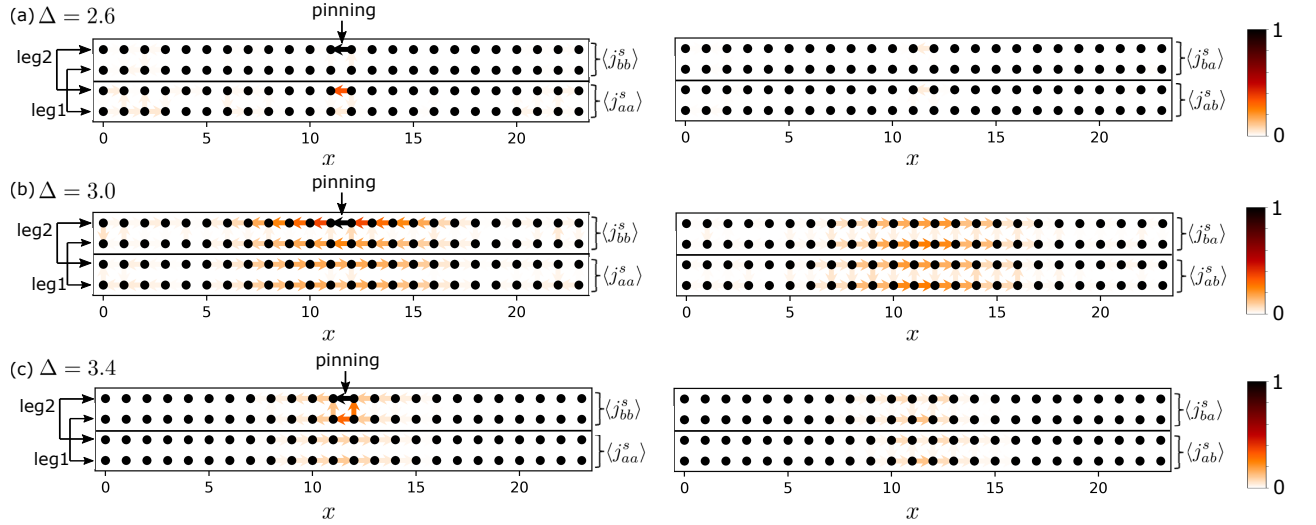


FIG. 1.  $\langle j_{\gamma\gamma'}^s(\mathbf{r}_{lm}) \rangle$  for the ETHM in the two-leg ladder with  $(L_x, L_y) = (24, 2)$  at electron density  $n = 1.92$  close to half filling. Their normalized magnitudes are shown by arrows with heatmap at the bond  $\mathbf{r}_{lm}$  for the intra-orbital ( $\gamma = \gamma'$ ) and inter-orbital ( $\gamma \neq \gamma'$ ) spin current in the left and right panels, respectively. Here, the legs of the ladder are labeled as leg 1 and leg 2, and the small pinning field is applied at the bond in leg 2 for orbital  $b$  (indicated by “pinning”). The model parameters are set to  $U = 4$ ,  $J_H = U/4$ ,  $(t_{aa}, t_{bb}) = (0.4, -0.2)$ , and  $t_{ab} = t_{ba} = 0.05$  with (a)  $\Delta = 2.6$ , (b)  $\Delta = 3$ , and (c)  $\Delta = 3.4$  in the unit of eV.

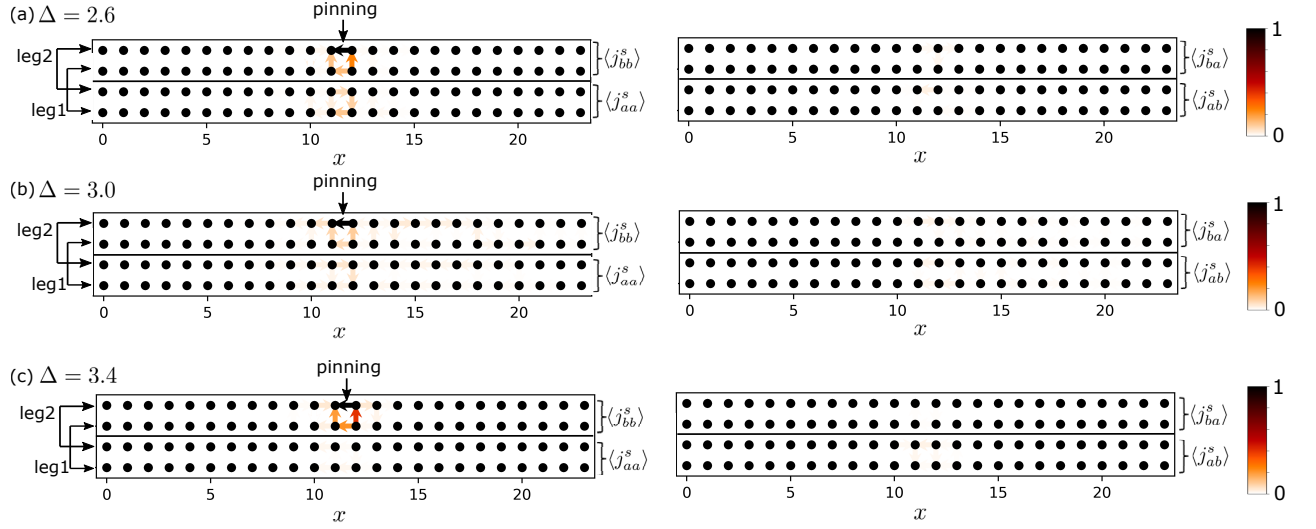


FIG. 2. Same as Fig. 1 but for  $t_{ab} = -t_{ba} = 0.05$ .

condensation in the spin channel, while the pair hopping is irrelevant. We also find that all off-diagonal parts of spin current  $\langle j_{ab}^s \rangle$  and  $\langle j_{ba}^s \rangle$ , shown in Fig. 1(b), flow in the same direction. At first glance, this behavior appears to be a spontaneous flow of global spin current. However, it turns out that the total spin current including both orbital diagonal and off-diagonal parts vanishes [60, 61], thus satisfying the Bloch theorem [68–71].

We can obtain sLC textures only when the even-type inter-orbital hoppings are introduced. In other words, no sLC textures emerge if the odd-type inter-orbital hoppings are introduced or no inter-orbital hoppings are introduced. Figure 2 shows the results of  $\langle j_{\gamma\gamma'}^s(\mathbf{r}_{lm}) \rangle$  for

the odd-type inter-orbital hoppings  $t_{ab} = -t_{ba} = 0.05$ . Indeed, we find that sLC textures are short-ranged. We also obtain almost the same results as in Fig. 2 when no inter-orbital hoppings are introduced. Therefore, the symmetry of the inter-orbital hoppings is a key factor in the generation of sLC textures. These features are in fact consistent with the previous work based on the (dynamical) mean-field theory [39, 60, 61], and thus we conclude that a sLC texture associated with an exciton condensation in the spin channel can occur in the ETHM. A candidate material realizing sLC textures is  $\text{Pr}_{0.5}\text{Ca}_{0.5}\text{CoO}_3$ , where an exciton condensation in the spin channel has been discussed [41].



## B. Carrier-doped orbital-selective Mott insulators

In the previous section, we have demonstrated that sLC textures emerge in the ETHM and shown that the inter-orbital hoppings play a crucial role in stabilizing sLC textures associated with exciton condensation in the spin channel. Here, in this section, we shall demonstrate that it is also possible to realize sLC textures in the ETHM without inter-orbital hoppings, i.e.,  $t_{ab} = t_{ba} = 0$ . For this purpose, we set the model parameters to be  $U = 3.5$ ,  $J_H = U/4$ ,  $\Delta = -1.6$ , and  $(t_{aa}, t_{bb}) = (-0.5, -0.15)$  in the unit of eV, which are used to describe orbital-selective Mott insulators such as  $\text{BaFe}_2\text{Se}_3$  [42]. As in Sec. III A, we consider the two-leg ladder with  $(L_x, L_y) = (24, 2)$ . Magnetic structures of this model have been investigated by the DMRG method and several types of block AFM order have been suggested [42].

We calculate the ground state of the ETHM by using the DMRG method, keeping  $\chi = 2500$  largest density-matrix eigenstates and taking 40 sweeps, which leads to a truncation error less than  $10^{-7}$ . Figures 3(a)–3(c) show the results of  $\langle j_{aa}^s(\mathbf{r}_{lm}) \rangle$  and  $\langle j_{bb}^s(\mathbf{r}_{lm}) \rangle$  for three different electron densities  $n = 2.5$ , 2.67, and 2.83. In these calculations, we introduce the pinning field at the bond of orbital  $b$  indicated in the figure. However, the following argument remains qualitatively the same even when the pinning field is applied to orbital  $a$ . At  $n = 2.5$ , a  $(\pi, 0)$  stripe order, i.e., AFM spin alignment along the legs and ferromagnetic (FM) spin alignment along the rungs, appears. Since the magnetic structure has already been studied [42], here we focus on the possibility of the emergence of sLC textures.

First, we do not find robust sLC textures for typical values of electron density in the range of  $2.0 \lesssim n \lesssim 2.5$  and  $n \sim 3$ . Indeed, the correlation of spin current is short-ranged, as shown in Fig. 3(a) for  $n = 2.5$  and Fig. 3(c) for  $n = 2.83$ . These features are better quantified by evaluating the Fourier transform of these quantities, i.e.,  $J_\gamma(\mathbf{q}) = \sum_{\mathbf{r}} \langle j_{\gamma\gamma}^s(\mathbf{r}) \rangle \cos(\mathbf{q} \cdot \mathbf{r})$ . As shown in Fig. 3(d) for  $n = 2.5$  and Fig. 3(f) for  $n = 2.83$ ,  $J_\gamma(\mathbf{q})$  has a structure around  $\mathbf{q} = (\pi, 0)$  and  $(0, 0)$ , respectively, but it is rather broad. In contrast, we find the enhanced signal of sLC textures in the range of electron density  $2.63 < n < 2.71$ , where the correlation of spin current is longer-ranged, as shown in Figs. 3(b) and 3(e) for  $n = 2.67$ .

We should note that the sLC textures found here are unaffected by the introduction of the inter-orbital hoppings  $t_{ab} = \pm t_{ba} = 0.05$  also used in Sec. III A, which indicates that the sLC textures found here in this section are due to a mechanism different from the exciton condensation in the spin channel. We also find that the introduction of  $\Delta \neq 0$  does not play an essential role. Since the sLC signal becomes small when the ratio of  $t_{bb}/t_{aa}$  is closer to 1, the difference in the itinerancy of electrons in orbitals  $a$  and  $b$  is related to the development of sLC textures.

Recalling that noncollinear magnetism can produce spin current [72], vector chirality is one of the possible origins for the sLC textures. It has been proposed in Ref. [46] that the correlation of vector chirality  $j_{bb}^{\text{ns}}(\mathbf{r}_{lm}) := (\mathbf{S}_{l,b} \times \mathbf{S}_{m,b})_z = S_{l,b}^x S_{m,b}^y - S_{l,b}^y S_{m,b}^x$  of localized spins on orbital  $b$  can be developed in the GKHM, which is an effective model of the ETHM in the strong coupling limit. Note that the vector chirality operator  $j_{bb}^{\text{ns}}(\mathbf{r}_{lm})$  is also regarded as a spin current operator defined on localized spins. It is also interesting to notice that the electron density  $n$  where sLC textures emerge is consistent for both models, i.e., the ETHM studied in this paper and the GKHM studied in Ref. [46]. However, the pattern of sLC textures is different between these two systems. In the ETHM, spin current flows in the leg direction for each orbital  $a$  or  $b$ , as shown in Fig. 3(b). Because spin currents in these two orbitals flow in opposite directions, the global spin current does not flow in total. In the GKHM, on the other hand, spin currents generated by itinerant electrons and by localized spins are inequivalent, which may thus induce another kind of sLC textures, i.e., staggered spin current circulating around  $2 \times 2$  plaquettes [46]. We have also examined  $j_{\gamma\gamma}^{\text{ns}}(\mathbf{r})$  in the ETHM and confirmed that the correlation of  $j_{\gamma\gamma}^{\text{ns}}(\mathbf{r})$  is developed when  $j_{\gamma\gamma}^s(\mathbf{r})$  exhibits enhanced correlation.

Finally, we note that the sLC textures found here in the ETHM coexist with charge stripes. Figure 4 shows the results of  $n_+^a(x) := \frac{1}{L_y} \sum_{y=1,2} (\langle n_{x,a}^y \rangle - n)$  and  $n_-^a(x) := \frac{1}{L_y} \sum_{y=1,2} [(-1)^y \langle n_{x,a}^y \rangle]$ , where  $n_{x,a}^y$  is an electron density operator at the  $x$ th rung ( $x = 1, 2, \dots, L_x$ ) for leg  $y$  and orbital  $a$ . These two quantities  $n_+^a(x)$  and  $n_-^a(x)$  represent respectively the average and difference of the numbers of electrons at legs 1 and 2 in each rung. When the sLC textures emerge, we find that charge stripes also appear probed in both  $n_+^a(x)$  and  $n_-^a(x)$ , as shown in Fig. 4 for  $n = 2.67$ , indicating the spontaneous formation of charge stripes both along rungs and legs. After removing the contributions from edges to reduce the finite-size effects, we find that  $\tilde{n}_+^a(q_x) := \sum_x n_+^a(x) \cos(q_x x)$  shows a peak structure at  $q_x \sim 2$  and similarly  $\tilde{n}_-^a(q_x) := \sum_x n_-^a(x) \cos(q_x x)$  shows a peak structure at  $q_x \sim 1$ , which correspond to charge stripes with the period of  $\lambda \simeq 3$  and 6 (in unit of the lattice constant), respectively. These charge stripes can trigger vector chirality when they form superlattice structures that break local inversion symmetry [73, 74]. Indeed, the emergence of antisymmetric exchange, i.e., the Dzyaloshinskii-Moriya interaction, has been proposed in ABC-type superlattices [75]. The coexistence of vector chirality and charge stripes is one manifestation of multiferroicity [72, 76]. We should also note that the coexistence of cLC textures and stripes has recently been reported in a spinless Hubbard model [38].

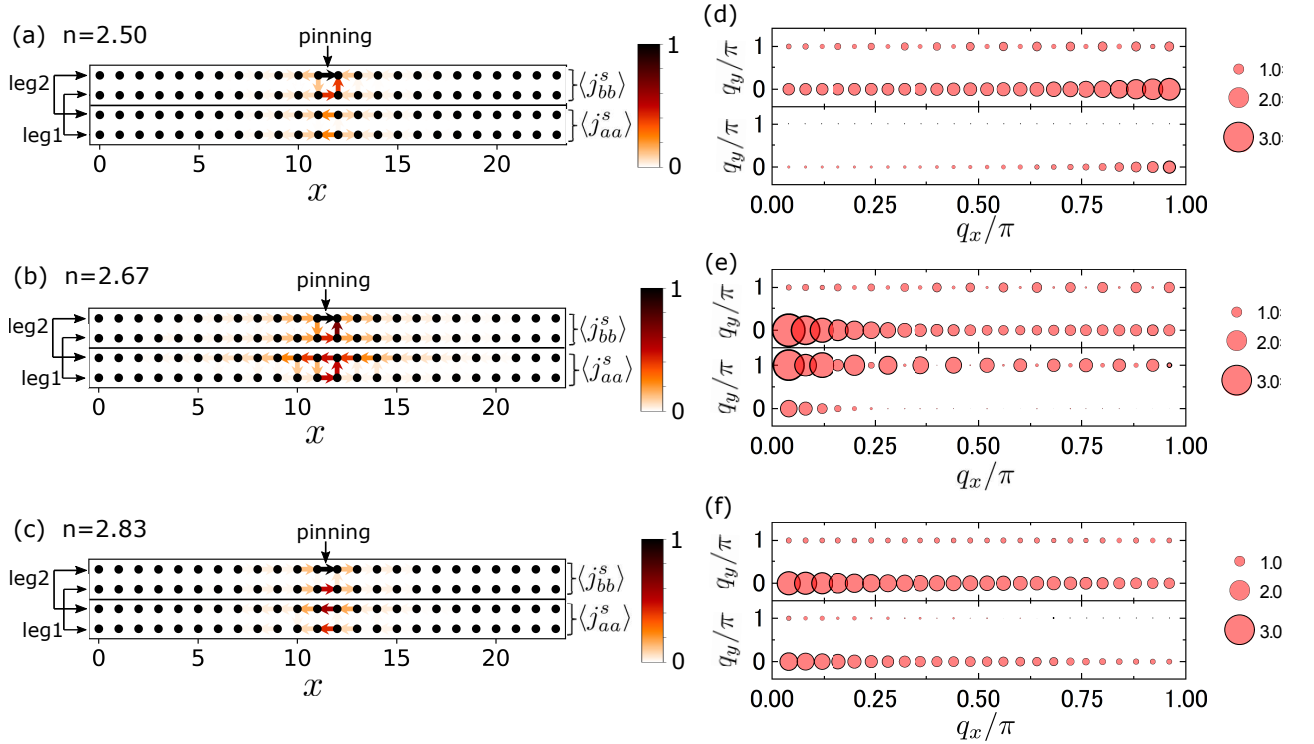


FIG. 3.  $\langle j_{\gamma\gamma'}^s(\mathbf{r}_{lm}) \rangle$  with  $\gamma = \gamma'$  for the ETHM in the two-leg ladder with  $(L_x, L_y) = (24, 2)$ . Their normalized magnitudes are shown by arrows with heatmap at the bond  $\mathbf{r}_{lm}$  for (a)  $n = 2.5$ , (b)  $n = 2.67$ , and (c)  $n = 2.83$ . Here, the legs of the ladder are labeled as leg 1 and leg 2, and the small pinning field is applied at the bond in leg 2 for orbital  $b$  (indicated by “pinning”). The model parameters are set to  $U = 3.5$ ,  $J_H = U/4$ ,  $(t_{aa}, t_{bb}) = (-0.5, -0.15)$ , and  $\Delta = -1.6$  in the unit of eV with the inter-orbital hoppings  $t_{ab} = t_{ba} = 0$ . In (d), (e), and (f),  $J_\gamma(\mathbf{q})$  are evaluated from the results shown in (a), (b), and (c), respectively. The diameter of the bubbles indicates the value of  $J_\gamma(\mathbf{q})$  at different momentum  $(q_x, q_y)$ . The lower and upper panels in each figure are for  $\langle j_{aa}^s(\mathbf{r}_{lm}) \rangle$  and  $\langle j_{bb}^s(\mathbf{r}_{lm}) \rangle$  or  $J_a(\mathbf{q})$  and  $J_b(\mathbf{q})$ , respectively.

#### IV. SINGLE-ORBITAL HUBBARD MODEL ON A SQUARE LATTICE

In Sec. III, we have demonstrated the emergence of sLC textures in the two-orbital Hubbard model on a ladder lattice. Even with only a single orbital, the two-dimensional Hubbard model exhibits very rich quantum phases with highly-entangled spin and charge degrees of freedom. In this section, we focus on sLC textures in the single-orbital Hubbard model on a square lattice. There are several proposals for sLC textures in the Hubbard model on a square lattice. In the Hubbard model with a single hole on a square lattice, the emergence of sLC textures has been suggested [77]. The sLC textures are driven by a many-body Berry-like phase, i.e., phase string [78–80] in the single-hole  $t$ - $J$  model on a square lattice. We should, however, note that total  $S^z$  is nonzero in Ref. [77], where time-reversal symmetry is explicitly broken in the Hamiltonian. Even for total  $S^z$  being zero, the recent theoretical analysis based on the functional renormalization group method in Ref. [40] has revealed the emergence of sLC textures in a hole-doped Hubbard model on a square lattice with further-neighbor hoppings. The sLC textures found in this analysis are characterized

with a wave vector  $\mathbf{q} = (\pi/2, \pi/2)$ , which is diagonal and closely related to the nesting vector of the Fermi surface [40].

Here, we investigate sLC textures in the single-orbital Hubbard model on a square lattice by using the DMRG method. The Hamiltonian of the Hubbard model on a square lattice is given as

$$\begin{aligned} \mathcal{H}_{t-t'-U} = & -t \sum_{\langle i,j \rangle, \tau} (c_{i,\tau}^\dagger c_{j,\tau} + \text{H.c.}) \\ & -t' \sum_{\langle\langle i,j \rangle\rangle, \tau} (c_{i,\tau}^\dagger c_{j,\tau} + \text{H.c.}) + U \sum_i n_{i,\uparrow} n_{i,\downarrow}, \end{aligned} \quad (7)$$

where  $c_{i,\tau}^\dagger$  is the electron creation operator at site  $i$  with spin  $\tau$  ( $=\uparrow, \downarrow$ ) and  $n_{i,\tau} = c_{i,\tau}^\dagger c_{i,\tau}$ .  $t$  and  $t'$  are nearest-neighbor and next-nearest-neighbor hoppings on a square lattice, respectively, and  $U$  is on-site Coulomb interaction. The sum indicated by  $\langle i, j \rangle$  ( $\langle\langle i, j \rangle\rangle$ ) runs over all pair of nearest-neighbor (next-nearest-neighbor) sites  $i$  and  $j$ .

We use a cluster of  $(L_x, L_y) = (8, 6)$  on a cylinder geometry, i.e., open and periodic boundary conditions along  $x$  and  $y$  axes, respectively. Although we can treat even

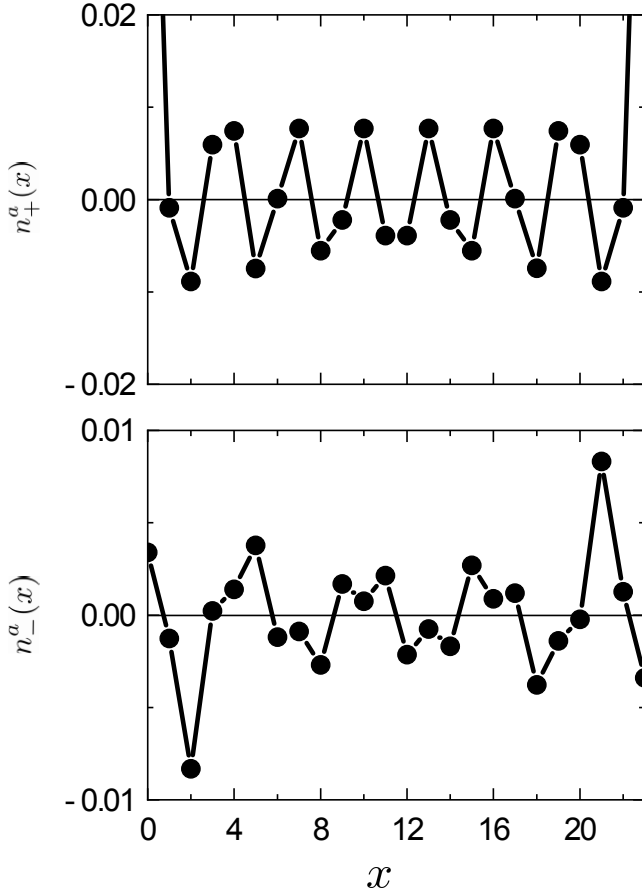


FIG. 4.  $n_+^a(x)$  (upper panel) and  $n_-^a(x)$  (lower panel) for the ETHM in the two-leg ladder with  $(L_x, L_y) = (24, 2)$  at  $n = 2.67$ . The model parameters are the same as those used in Fig. 3

larger clusters at the expense of accuracy, we avoid using too large clusters since the high computational accuracy is required to correctly calculate off-diagonal quantities such as spin current. To treat a two-dimensional cluster in the DMRG method, we construct a snakelike one-dimensional chain out of the two-dimensional square lattice, running from site at  $(0, 0)$  to site at  $(0, L_y - 1)$ , then from site at  $(1, L_y - 1)$  to site at  $(1, 0)$ , and this pattern being repeated until we reach site at  $(L_x - 1, 0)$ . We keep  $\chi = 10000$  largest density-matrix eigenstates and take 40 sweeps in the DMRG calculations, leading to a truncation error less than  $5 \times 10^{-5}$ .

Similar to Eq. (6), the spin current operator for the single-band Hubbard model is defined as

$$j^s(\mathbf{r}_{lm}) := i(\text{sgn } t \text{ or } t') \sum_{\tau} \frac{s_{\tau}}{2} \left( c_{l,\tau}^{\dagger} c_{m,\tau} - c_{m,\tau}^{\dagger} c_{l,\tau} \right) \quad (8)$$

for a bond  $(l, m)$  connecting sites  $l$  and  $m$  denoted as  $\mathbf{r}_{lm}$ . To investigate the spin current, we introduce a small pinning field  $j^s(\mathbf{r}_{lm})$  on a bond  $(l, m)$ , described by  $\mathcal{H}^s = -h|t|j^s(\mathbf{r}_{lm})$  with  $h = 0.0001$ , i.e., site  $l$  located at  $(0, 2)$  and site  $m$  located at  $(0, 3)$  for our cluster with  $(L_x, L_y) = (8, 6)$  (also see Fig. 5).

Figure 5 summarizes the results of  $\langle j^s(\mathbf{r}_{lm}) \rangle$  for  $t'/t = -0.3$  and  $U/t = 9$  with different hole concentrations  $\delta = 1 - n$ . We find that the correlation of  $\langle j^s(\mathbf{r}_{lm}) \rangle$  is rather short-ranged except for  $\delta = 0.125$ . Note that half filling is achieved at  $n = 1$  for the single-orbital Hubbard model. We also note that the global spin current in the  $x$  direction should be zero due to the open boundary conditions, whereas the spin current in the  $y$  direction should be suppressed by  $L_y^{-1}$  due to the periodic boundary conditions [71].

In addition to the hole concentration, several other conditions are required for the emergence of the sLC textures. Figure 6 shows the results of  $\langle j^s(\mathbf{r}_{lm}) \rangle$  for different values of  $t'$  at  $\delta = 0.125$ , revealing that the presence of  $t'/t \sim -0.25$  is necessary to induce the robust sLC textures. Figures 7(a)–7(c) show the results of  $\langle j^s(\mathbf{r}_{lm}) \rangle$  for three different values of  $U/t = 4, 6$ , and  $9$  at  $\delta = 0.125$  and  $t'/t = -0.266$ . These results clearly find that the sLC textures are most extended and enhanced when  $U/t$  is smaller. Figures 7(d)–7(f) show  $J(\mathbf{q}) = \sum_{\mathbf{r}} \langle j^s(\mathbf{r}) \rangle \cos(\mathbf{q} \cdot \mathbf{r})$  evaluated from the results of  $\langle j^s(\mathbf{r}_{lm}) \rangle$  in Figs. 7(a)–7(c). We find that the centroid of  $J(\mathbf{q})$  is concentrated toward  $\mathbf{q} \simeq (\pi, 0)$  with decreasing  $U/t$ . We should also note that even when  $U/t = 4$ , no sLC textures emerge if  $t'/t$  deviates significantly away from  $-0.25$ .

It is interesting to compare the sLC texture obtained here by the DMRG method with those reported in Ref. [40]. Based on the functional-renormalization group method, the presence of sLC textures has been proposed in the single-orbital Hubbard model with  $t'/t = -1/6$ ,  $t''/t = 1/5$ , and  $U/t = 3.3$  at  $\delta = 0.2$ , where  $t''$  is the third nearest-neighbor hopping [40]. The suggested sLC textures are characterized by wave vector  $\mathbf{q} \simeq (\pi/2, \pi/2)$ . The similarity and difference of the results by our study and their study [40] are summarized as follows. Both studies suggest that the introduction of relatively small or intermediate  $U/t$  and  $t'/t$  is crucial for the emergence of the robust sLC textures. However, the sLC textures appear most significantly at  $\delta = 0.125$  in our study but at  $\delta = 0.2$  in their study. The wave vector  $\mathbf{q}$  characterizing the spatial pattern of sLC textures is also different: while the axial-sLC textures with  $\mathbf{q} = (\pi, 0)$  are found by our DMRG study, the diagonal-sLC textures with  $(\pi/2, \pi/2)$  are obtained by their functional renormalization group study [40]. The axial-sLC textures may be stabilized here because we employ the cluster of a cylinder geometry. However, more detailed study is deserved to clarify this point.

Now we comment on the coexistence of sLC textures and charge stripes at  $\delta = 0.125$ . The hole density of  $\delta = 0.125$  is well-known as the density at which the charge stripes appear, and many previous studies have been focused on this density [81–93]. In the Hubbard model in the strong coupling region or the  $t$ - $J$  model on a 4-leg ladder under the cylinder geometry, the axial charge stripes with a period of  $\lambda = 8$  (in unit of the lattice constant) characterized by its ordering wave vector

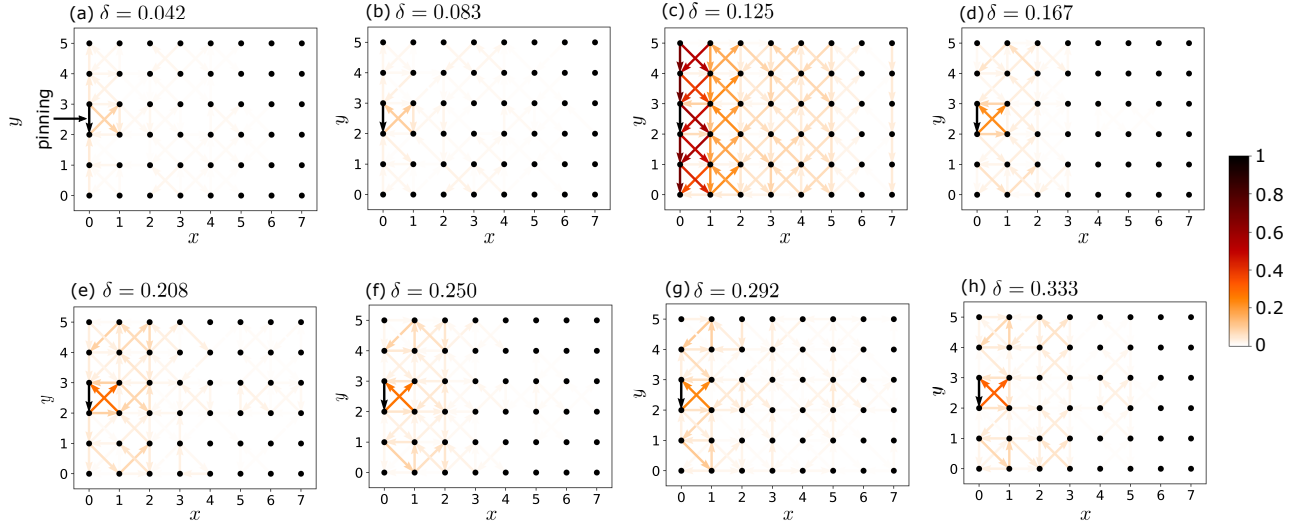


FIG. 5.  $\langle j^s(\mathbf{r}_{lm}) \rangle$  for the single-orbital Hubbard model with  $U/t = 9$  and  $t'/t = -0.3$  on the square lattice with  $(L_x, L_y) = (8, 6)$ . Their normalized amplitudes are shown by arrows with heatmap at the bond  $\mathbf{r}_{lm}$  for (a)  $\delta = 0.042$ , (b)  $\delta = 0.083$ , (c)  $\delta = 0.125$ , (d)  $\delta = 0.167$ , (e)  $\delta = 0.208$ , (f)  $\delta = 0.250$ , (g)  $\delta = 0.292$ , and (h)  $\delta = 0.333$ . Here, the bond to which the small pinning field is applied is indicated by “pinning” in (a). The same pinning field is also applied in (b)–(h), but it is not explicitly indicated.

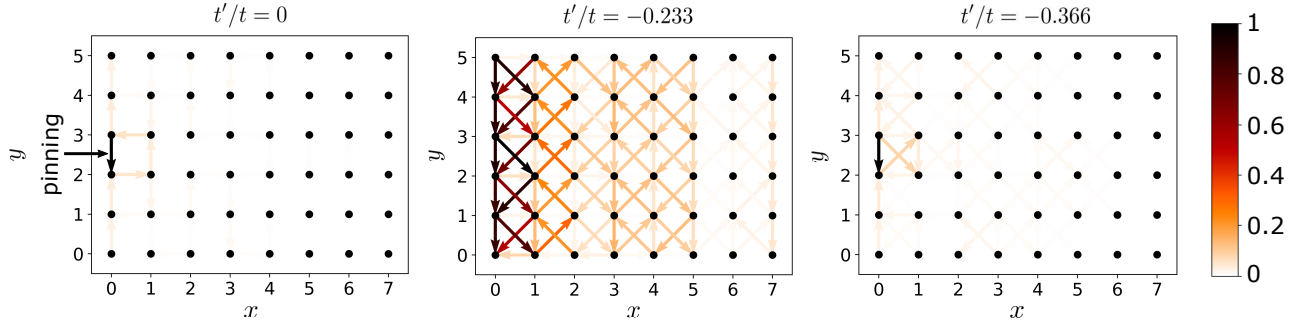


FIG. 6. Same as Fig. 5 but for three different  $t'$  values (indicated in the figures) at  $\delta = 0.125$

$\mathbf{q} = (\pi/4, 0)$  is stabilized at  $\delta = 0.125$  [90]. Introducing  $t'/t = -0.25$ , the  $\lambda = 4$  charge stripes with its ordering wave vector  $\mathbf{q} = (\pi/2, 0)$  appears. Here we shall show that the charge stripes also appear on the 6-leg ladder used in this section.

In order to quantify the charge distribution along the  $x$  axis, i.e., the leg direction, we evaluate  $n(x) := \frac{1}{L_y} \sum_{y=0}^{L_y-1} \langle n_x^y \rangle$ , where  $n_x^y$  is an electron density operator at the  $x$ th rung ( $x = 0, 1, \dots, L_x - 1$ ) in leg  $y$ . Since the computation of diagonal quantities such as the charge density is not severely sensitive to the lower accuracy in the DMRG method, we can evaluate this quantity  $n(x)$  for a larger cluster with  $(L_x, L_y) = (16, 6)$ . Since the cluster is on a cylinder geometry, we expect that the axial charge stripes are more stable. We indeed find in Fig. 8 that the axial charge stripes appear at  $\delta = 0.125$  and the period of these stripes become longer with decreasing  $U$ .

To further discuss the period of the charge stripes, we also evaluate  $n(q_x) := \sum_x n(x) \cos(q_x x)$  and the results are shown in Fig. 9. As shown in Fig. 9(a), when

$t'/t = -0.3$  and  $U/t = 4$ ,  $n(q_x)$  has a broad peak at  $0.32 \lesssim q_x/\pi \lesssim 0.80$  for the cluster with  $(L_x, L_y) = (8, 6)$ . We can reduce the finite size effect when we consider the cluster with  $(L_x, L_y) = (16, 6)$ , for which the results of  $n(q_x)$  are shown in Figs. 9(b)–9(d) for three different values of  $U/t = 4, 6$ , and  $9$ . As shown in Fig. 9(b), when  $t'/t = -0.3$  and  $U/t = 4$ ,  $n(q_x)$  exhibits a peak at  $0.25 \lesssim q_x/\pi \lesssim 0.48$ , which indicates the charge stripes with  $\lambda \simeq 5$ . This is consistent with the results obtained by the variational Monte-Carlo study on a 6-leg Hubbard ladder with  $t'$  [93]. With increasing  $U$ , the characteristic ordering wave vector of the charge stripes becomes larger, as shown in Fig. 9(d) for  $U/t = 9$ , where  $n(q_x)$  has a peak at  $0.45 \lesssim q_x/\pi \lesssim 0.60$ , leading to  $\lambda \simeq 4$ . Since  $\delta = 0.125$  is a key factor in the development of the sLC textures, it is most likely that the presence of charge stripes is crucial for the emergence of the sLC textures found here. Assuming that a symmetry breaking leads to the emergent spin-orbit coupling as discussed in Sec. II, the electric field produced locally by charge stripes may



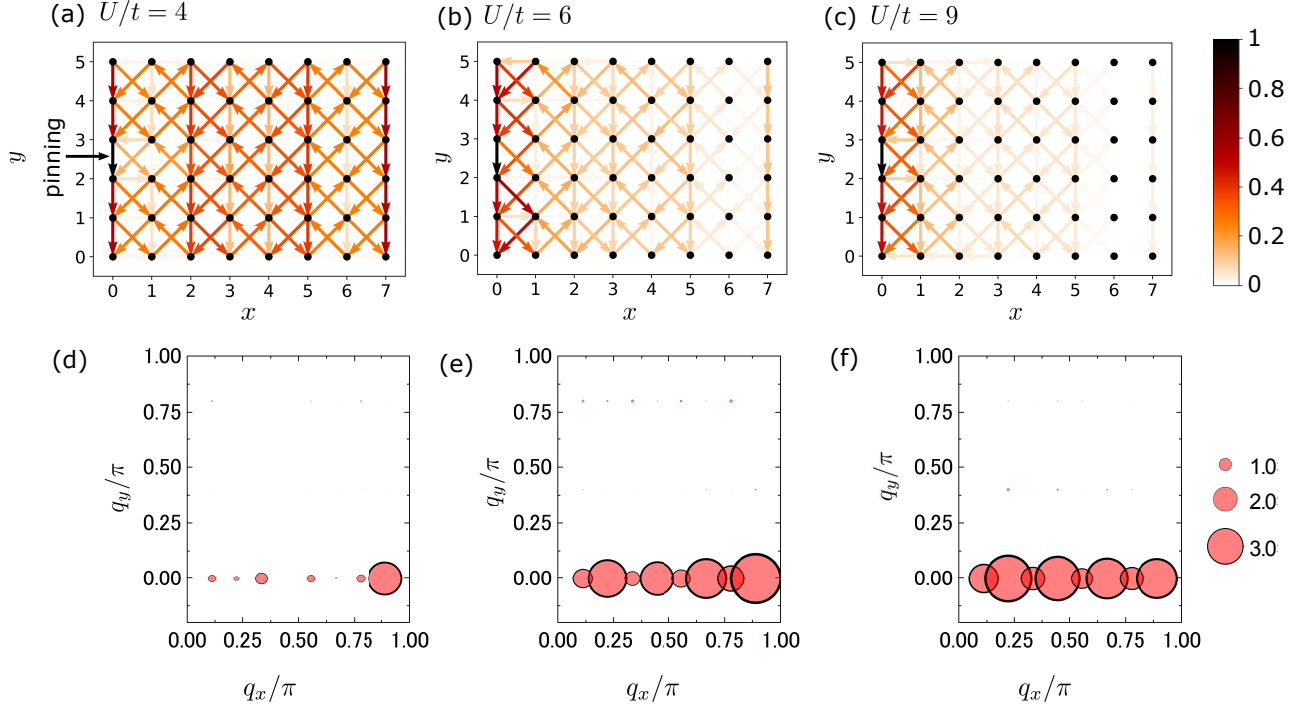


FIG. 7. (a)–(c) Same as Fig. 5 but for (a)  $U/t = 4$ , (b)  $U/t = 6$ , and (c)  $U/t = 9$  at  $\delta = 0.125$  and  $t'/t = -0.266$ . (d)–(f)  $J(\mathbf{q})$  evaluated from  $\langle j^s(\mathbf{r}_{lm}) \rangle$  shown in (a)–(b), i.e., for (d)  $U/t = 4$ , (e)  $U/t = 6$ , and (f)  $U/t = 9$ . The diameters of bubbles indicate the values of  $J(\mathbf{q})$ .

induce spin current by a similar mechanism to the spin Hall effect [94, 95].

## V. SUMMARY

We have studied sLC textures emerging in the ground states of the Hubbard models by using the DMRG method. Particularly, we have investigated carrier-doped (i) excitonic insulators, (ii) orbital-selective Mott insulators, and (iii) two-dimensional Mott insulators, modeled by the ETHM on a two-leg ladder lattice in (i) and (ii), and the single-orbital Hubbard model with the next-nearest hopping  $t'$  on a square lattice in (iii). In these systems, we have obtained the enhanced sLC textures developed around a bond to which the pinning field is applied.

In system (i), we have found the emergence of sLC textures which is associated with exciton condensation in the spin channel. Using typical model parameters for cobalt oxides such as  $\text{Pr}_{0.5}\text{Ca}_{0.5}\text{CoO}_3$ , we have found that the sLC correlations are developed most significantly near half-filling at electron density  $n = 1.92$  when the crystal field and the inter-orbital hoppings are suitably introduced. In system (ii), we have used typical model parameters for iron oxides such as  $\text{BaFe}_2\text{Se}_3$  and found that the robust sLC textures emerge in the ETHM without introducing inter-orbital hoppings. The sLC textures are developed most profoundly when a relatively large

number of carriers is introduced in the range of electron density  $2.63 < n < 2.71$  and the difference in itinerancy of electrons in the two orbitals is large. We have also found that the sLC textures coexist with the charge stripes formed in both rungs and legs. In system (iii), we have found that the sLC textures are most enhanced and extended at  $\delta = 0.125$  when  $t'/t \sim -0.25$  is introduced. We also found that the sLC textures are most developed when  $U$  decreases from  $U/t = 9$  to  $U/t = 4$ . The charge stripes also simultaneously appear when the sLC textures emerge.

In conclusion, we have found the conditions under which the sLC textures are developed in each of the three systems (i)–(iii). Our results clearly demonstrate that quantum many-body effects can induce local spin current in the ground state. It is interesting to explore whether the sLC textures can lead to the development of spintronics in strongly correlated electron systems. Finally, we note that the ground states with only short-ranged cLC correlations have been found in all three systems (i)–(iii).

## ACKNOWLEDGMENTS

This work was supported by Grant-in-Aid for Scientific Research (B) (Nos. 19H01829, 19H05825, 20H01849, and 21H03455) and Grant-in-Aid for Early-Career Scientists (No. JP23K13066) from Ministry of Education, Cul-

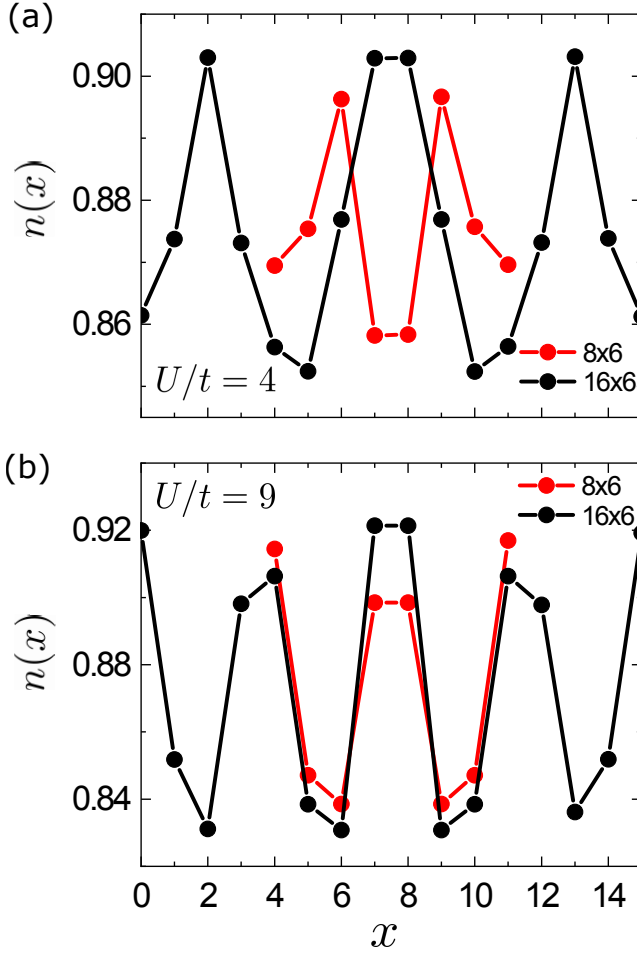


FIG. 8. Charge density averaged over sites along the  $y$  direction,  $n(x)$ , for the single-orbital Hubbard model with  $t'/t = -0.266$  at  $\delta = 0.125$  on the square lattices with  $(L_x, L_y) = (8, 6)$  (red dots) and  $(L_x, L_y) = (16, 6)$  (black dots). The on-site Coulomb interaction is set to (a)  $U/t = 4$  and (b)  $U/t = 9$ . For easier comparison, the results for  $(L_x, L_y) = (8, 6)$  are displaced by 4 in the horizontal axis.

ture, Sports, Science, and Technology (MEXT), Japan, and by JST PRESTO (Grant No. JPMJPR2013). This work was also supported in part by the COE research grant in computational science from Hyogo Prefecture and Kobe City through Foundation for Computational Science. Numerical calculation was carried out using the HOKUSAI supercomputer at RIKEN, computational resources of the facilities of the Supercomputer Center at Institute for Solid State Physics, the University of Tokyo, and the supercomputer system at the information initiative center, Hokkaido University through the HPCI System Research Project (Project ID: hp220049).

- 
- [1] A. Kivelson, E. Fradkin, and V. J. Emery, Electronic liquid-crystal phases of a doped Mott insulator, *Nature* (London) **393**, 550 (1998).
  - [2] A. Kivelson, I. P. Bindloss, E. Fradkin, V. Oganesyan, J. M. Tranquada, A. Kapitulnik, and C. Howald, How to detect fluctuating stripes in the high-temperature superconductors, *Rev. Mod. Phys.* **75**, 1201 (2003).
  - [3] M. Vojta, Lattice symmetry breaking in cuprate superconductors: Stripes, nematics, and superconductivity, *Adv. Phys.* **58**, 699 (2009).
  - [4] E. Fradkin, S. A. Kivelson, M. J. Lawler, J. P. Eisenstein, and A. P. Mackenzie, Nematic Fermi Fluids in Condensed Matter Physics, *Annu. Rev. Condens. Matter Phys.* **1**, 153 (2010).
  - [5] E. Fradkin, *Electronic Liquid Crystal Phases in Strongly Correlated Systems*, *Lecture Notes in Physics Vol. 843* edited by D. C. Cabra, A. Honecker, and P. Pujol (Springer-Verlag, 2012), p. 53.
  - [6] E. Fradkin, S. A. Kivelson, and J. M. Tranquada, Colloquium: Theory of intertwined orders in high temperature superconductors, *Rev. Mod. Phys.* **87**, 457 (2015).
  - [7] H. Yamase and H. Kohno, Instability toward Formation of Quasi-One-Dimensional Fermi Surface in Two-Dimensional  $t$ - $J$  Model, *J. Phys. Soc. Jpn.* **69**, 2151 (2000).
  - [8] C. J. Halboth and W. Metzner,  $d$ -Wave Superconductivity and Pomeranchuk Instability in the Two-Dimensional Hubbard Model, *Phys. Rev. Lett.* **85**, 5162 (2000).
  - [9] V. Oganesyan, S. A. Kivelson, and E. Fradkin, Quantum Theory of a Nematic Fermi Fluid, *Phys. Rev. B* **64**, 195109 (2001).
  - [10] W. Metzner, D. Rohe, and S. Andergassen, Soft Fermi surfaces and breakdown of Fermi-liquid behavior, *Phys. Rev. Lett.* **91**, 066402 (2003).

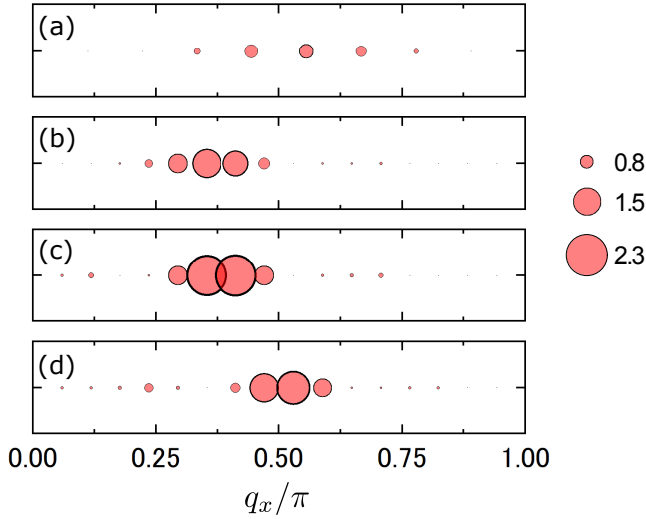


FIG. 9.  $n(q_x)$  for the single-orbital Hubbard model with  $t'/t = -0.266$  at  $\delta = 0.125$ . The diameters of bubbles indicate the magnitudes of  $n(q_x)$ . (a)  $U/t = 4$  on the square lattice with  $(L_x, L_y) = (8, 6)$ , and (b)  $U/t = 4$ , (c)  $U/t = 6$ , and (d)  $U/t = 9$  on the square lattice with  $(L_x, L_y) = (16, 6)$ .

[11] H. Y. Kee, E. Kim, and C. H. Chung, Signatures of an electronic nematic phase at the isotropic-nematic phase transition, *Phys. Rev. B*, **68**, 245109 (2003).  
[12] H.-Y. Kee, H. Doh, and T. Grzesiak, Intimate relations between electronic nematic, d-density wave and d-wave superconducting states, *J. Phys. Condens. Matter* **20**, 255248 (2008).  
[13] B. I. Halperin and T. M. Rice, *The Excitonic State at the Semiconductor-Semimetal Transition*, Solid State Physics (Academic Press, New York, 1968), p. 115.  
[14] I. Affleck and J. B. Marston, Large- $n$  limit of the Heisenberg-Hubbard model: Implications for high- $T_c$  superconductors, *Phys. Rev. B* **37**, 3774 (1988).  
[15] J. B. Marston and I. Affleck, Large- $n$  limit of the Hubbard-Heisenberg model, *Phys. Rev. B* **39**, 11538 (1989).  
[16] A. A. Nersisyan and G.E. Vachnadze, Low-Temperature Thermodynamics of the Two-Dimensional Orbital Antiferromagnet, *J. Low Temp. Phys.* **77**, 293 (1989).  
[17] H. J. Schulz, Fermi-surface instabilities of a generalized two-dimensional Hubbard model, *Phys. Rev. B* **39**, 2940 (1989).  
[18] J. Jeong, Y. Sidis, A. Louat, V. Brouet, and P. Bourges, Time-reversal symmetry breaking hidden order in  $\text{Sr}_2(\text{Ir,Rh})\text{O}_4$ , *Nature Comm.* **8**, 15119 (2017).  
[19] H. Murayama, K. Ishida, R. Kurihara, T. Ono, Y. Sato, Y. Kasahara, H. Watanabe, Y. Yanase, G. Cao, Y. Mizukami, T. Shibauchi, Y. Matsuda, and S. Kasahara, Bond Directional Anapole Order in a Spin-Orbit Coupled Mott Insulator  $\text{Sr}_2(\text{Ir}_{1-x}\text{Rh}_x)\text{O}_4$ , *Phys. Rev. X* **11**, 011021 (2021).  
[20] L. Mangin-Thro, Y. Sidis, A. Wildes, and P. Bourges, Intra-unit-cell magnetic correlations near optimal doping in  $\text{YBa}_2\text{Cu}_3\text{O}_{6.85}$ , *Nat. Commun.* **6**, 7705 (2015).  
[21] L. Zhao, C. A. Belvin, R. Liang, D. A. Bonn, W. N. Hardy, N. P. Armitage, and D. Hsieh, A global inversion-symmetry-broken phase inside the pseudogap region of

$\text{YBa}_2\text{Cu}_3\text{O}_y$ , *Nat. Phys.* **13**, 250 (2017).  
[22] D. Bounoua, D. Bounoua, L. Mangin-Thro, J. Jeong, R. Saint-Martin, L. Pinsard-Gaudart, Y. Sidis, and P. Bourges, Loop currents in two-leg ladder cuprates, *Commun. Phys.* **3**, 123 (2020).  
[23] D. J. Scalapino, S. R. White, and I. Affleck, Rung-rung current correlations on a 2-leg  $t$ - $J$  ladder, *Phys. Rev. B* **64**, 100506(R) (2001).  
[24] M. Greiter and R. Thomale, No Evidence for Spontaneous Orbital Currents in Numerical Studies of Three-Band Models for the  $\text{CuO}$  Planes of High Temperature Superconductors, *Phys. Rev. Lett.* **99**, 027005 (2007).  
[25] R. Thomale and M. Greiter, Numerical analysis of three-band models for  $\text{CuO}$  planes as candidates for a spontaneous T-violating orbital current phase, *Phys. Rev. B* **77**, 094511 (2008).  
[26] S. Nishimoto, E. Jeckelmann, and D. J. Scalapino, Current-current correlations in the three-band model for two-leg  $\text{CuO}$  ladders: Density-matrix renormalization group study, *Phys. Rev. B* **79**, 205115 (2009).  
[27] Y. F. Kung, C.-C. Chen, B. Moritz, S. Johnston, R. Thomale, and T. P. Devereaux, Numerical exploration of spontaneous broken symmetries in multiorbital Hubbard models, *Phys. Rev. B* **90**, 224507 (2014).  
[28] C. M. Varma, Non-Fermi-liquid states and pairing instability of a general model of copper oxide metals, *Phys. Rev. B* **55**, 14554 (1997).  
[29] S. Chakravarty, R. B. Laughlin, D. K. Morr, and C. Nayak, Hidden order in the cuprates, *Phys. Rev. B* **63**, 094503 (2001).  
[30] C. M. Varma, Cure to the Landau-Pomeranchuk and associated long-wavelength Fermi-surface instabilities on the lattice, *Philos. Mag.* **85**, 1657 (2005).  
[31] X.-G. Wen and P. A. Lee, Theory of Underdoped Cuprates, *Phys. Rev. Lett.* **76**, 503 (1996).  
[32] J. B. Marston, J. O. Fjærestad, and A. Sudbø, Staggered Flux Phase in a Model of Strongly Correlated Electrons, *Phys. Rev. Lett.* **89**, 056404 (2002).  
[33] U. Schollwöck, S. Chakravarty and J. O. Fjærestad, J. B. Marston, and M. Troyer, Broken Time-Reversal Symmetry in Strongly Correlated Ladder Structures, *Phys. Rev. Lett.* **90**, 186401 (2003).  
[34] C. Wu, W. V. Liu, and E. Fradkin, Competing orders in coupled Luttinger liquids, *Phys. Rev. B* **68**, 115104 (2003).  
[35] J.O. Fjærestad, J.B. Marston, and U. Schollwöck, Orbital currents and charge density waves in a generalized Hubbard ladder, *Annals of Physics* **321**, 894 (2006).  
[36] S. Sur, S.-S. Gong, K. Yang, and O. Vafek, Quantum anomalous Hall insulator stabilized by competing interactions, *Phys. Rev. B* **98**, 125144 (2018).  
[37] S. Julià-Farré, M. Müller, M. Lewenstein, and A. Dauphin, Self-Trapped Polarons and Topological Defects in a Topological Mott Insulator, *Phys. Rev. Lett.* **125**, 240601 (2020).  
[38] S. Julià-Farré, L. Cardarelli, M. Lewenstein, M. Müller, and A. Dauphin, Topological stripe state in an extended Fermi-Hubbard model, *arXiv*: 2301.03312.  
[39] J. Kuneš and D. Geffroy, Spontaneous Spin Textures in Multiorbital Mott Systems, *Phys. Rev. Lett.* **116**, 256403 (2016).  
[40] H. Kontani, Y. Yamakawa, R. Tazai, and S. Onari, Odd-parity spin-loop-current order mediated by transverse spin fluctuations in cuprates and related electron sys-

- tems, Phys. Rev. Res. **3**, 013127 (2021).
- [41] J. Kuneš and P. Augustinský, Excitonic condensation of strongly correlated electrons: The case of  $\text{Pr}_{0.5}\text{Ca}_{0.5}\text{CoO}_3$ , Phys. Rev. B **90**, 235112 (2014).
  - [42] J. Herbrych, J. Heverhagen, N. D. Patel, G. Alvarez, M. Daghofer, A. Moreo, and E. Dagotto, Novel Magnetic Block States in Low-Dimensional Iron-Based Superconductors, Phys. Rev. Lett. **123**, 027203 (2019).
  - [43] M. Mourigal, Shan Wu, M. B. Stone, J. R. Neilson, J. M. Caron, T. M. McQueen, and C. L. Broholm, Block Magnetic Excitations in the Orbitaly Selective Mott Insulator  $\text{BaFe}_2\text{Se}_3$ , Phys. Rev. Lett. **115**, 047401 (2015).
  - [44] S. Chi, Y. Uwatoko, H. Cao, Y. Hirata, K. Hashizume, T. Aoyama, and K. Ohgushi, Magnetic Precursor of the Pressure-Induced Superconductivity in Fe-Ladder Compounds, Phys. Rev. Lett. **117**, 047003 (2016).
  - [45] J. M. Caron, J. R. Neilson, D. C. Miller, K. Arpino, A. Llobet, and T. M. McQueen, Orbital-selective magnetism in the spin-ladder iron selenides  $\text{Ba}_{1-x}\text{K}_x\text{Fe}_2\text{Se}_3$ , Phys. Rev. B **85**, 180405(R) (2012).
  - [46] M. Środa, E. Dagotto, and J. Herbrych, Quantum magnetism of iron-based ladders: Blocks, spirals, and spin flux, Phys. Rev. B **104**, 045128 (2021).
  - [47] I. I. Pomeranchuk, On the stability of a Fermi liquid, Sov. Phys. JETP **8**, 361 (1958).
  - [48] G. Baym and C. Pethick, Landau Fermi-Liquid Theory, Jonh Wiley and Sons., Inc. New York and Toronto, 1992.
  - [49] A. J. Leggett, Quantum Liquids: Bose condensation and Cooper pairing in condensed-matter systems (Oxford Univ. Press, Oxford, 2006).
  - [50] C. Wu, K. Sun, E. Fradkin, and S.-C. Zhang, Fermi liquid instabilities in the spin channel, Phys. Rev. B **75**, 115103 (2007).
  - [51] C. Wu and S.-C. Zhang, Dynamic Generation of Spin-Orbit Coupling, Phys. Rev. Lett. **93**, 036403 (2004).
  - [52] A. J. Leggett, A theoretical description of the new phases of liquid  $^3\text{He}$ , Rev. Mod. Phys. **47**, 331 (1975).
  - [53] E. Rashba, Properties of semiconductors with an extremum loop. I. Cyclotron and combinational Resonance in a magnetic field perpendicular to the plane of the loop, Sov. Phys. Solid State **2**, 1109 (1960).
  - [54] G. Dresselhaus, Spin-Orbit Coupling Effects in Zinc Blende Structures, Phys. Rev. **100**, 580 (1955).
  - [55] S. Raghu, X.-L. Qi, C. Honerkamp, and S.-C. Zhang, Topological Mott Insulators, Phys. Rev. Lett. **100**, 156401 (2008).
  - [56] N. F. Mott, The transition to the metallic state, Philos. Mag. **6**, 287 (1961).
  - [57] R. S. Knox, Theory of Excitons (Supplement 5 to Solid State Physics, ed. by F. Seitz and D. Turnbull, Academic Press, N. Y., 1963).
  - [58] L. V. Keldysh and Y. V. Kopayev, Possible instability of semimetallic state toward Coulomb interaction, Sov. Phys. Solid State **6**, 2219 (1965).
  - [59] B. I. Halperin and T. M. Rice, Possible Anomalies at a Semimetal-Semiconductor Transistion, Rev. Mod. Phys. **40**, 755 (1968).
  - [60] D. Geffroy, A. Hariki, and J. Kuneš, Excitonic magnet in external field: Complex order parameter and spin currents, Phys. Rev. B **97**, 155114 (2018).
  - [61] H. Nishida, S. Miyakoshi, T. Kaneko, K. Sugimoto, and Y. Ohta, Spin textures and spin current in excitonic phases of the two-band Hubbard model, Phys. Rev. B **99**, 035119 (2019).
  - [62] T. Kaneko and Y. Ohta, Roles of Hund's rule coupling in excitonic density-wave states, Phys. Rev. B **90**, 245144 (2014).
  - [63] J. Kuneš and P. Augustinský, Excitonic instability at the spin-state transition in the two-band Hubbard model, Phys. Rev. B **89**, 115134 (2014).
  - [64] S. R. White, and A. L. Chernyshev, Néel order in square and triangular lattice Heisenberg models, Phys. Rev. Lett. **99**, 127004 (2007).
  - [65] M. Qin, C.-M. Chung, H. Shi, E. Vitali, C. Hubig, U. Schollwöck, S. R. White, and S. Zhang, Absence of Superconductivity in the Pure Two-Dimensional Hubbard Model, Phys. Rev. X **10**, 031016 (2020).
  - [66] S. Jiang, D. J. Scalapino, and S. R. White, Ground-state phase diagram of the  $t$ - $t'$ - $J$  model, PNAS **118**, e2109978118 (2021).
  - [67] Due to the introduction of nonzero pair hoppings, the value of  $\Delta$  for which the exciton condensation appears is shifted from  $\Delta = 3.4$  reported in the previous study without pair hoppings [39].
  - [68] L. Brillouin, Le champ self-consistent, pour des électrons liés; la supraconductibilité, J. De Phys. Et Rad. **4**, 334 (1933).
  - [69] H. Grayson Smith and J. O. Wilhelm, Superconductivity, Rev. Mod. Phys. **7**, 237 (1935).
  - [70] D. Bohm, Note on a Theorem of Bloch Concerning Possible Causes of Superconductivity, Phys. Rev. **75**, 502 (1949).
  - [71] H. Watanabe, A Proof of the Bloch Theorem for Lattice Models, J. Stat. Phys. **177**, 717 (2019).
  - [72] H. Katsura, N. Nagaosa, and A. V. Balatsky, Spin Current and Magnetoelectric Effect in Noncollinear Magnets, Phys. Rev. Lett. **95**, 057205 (2005).
  - [73] X. Zhang, Q. Liu, J.-W. Luo, A. J. Freeman, and A. Zunger, Hidden spin polarization in inversion-symmetric bulk crystals, Nat. Phys. **10**, 387 (2014).
  - [74] M. H. Fischer, M. Sigrist, D. F. Agterberg, and Y. Yanase, Superconductivity and Local Inversion-Symmetry Breaking, Annu. Rev. Condens. Matter Phys. **14**, 153 (2023).
  - [75] W. S. Ham, A.-M. Pradipto, K. Yakushiji, K. Kim, S. H. Rhim, K. Nakamura, Y. Shiota, S. Kim, and T. Ono, Dzyaloshinskii-Moriya interaction in noncentrosymmetric superlattices, npj Comput. Mater. **7**, 129 (2021).
  - [76] S.-W. Cheong and M. Mostovoy, Multiferroics: a magnetic twist for ferroelectricity, Nature Mater. **6**, 13 (2007).
  - [77] W. Zheng, Z. Zhu, D. N. Sheng, and Z. Y. Weng, Hidden spin current in doped Mott antiferromagnets, Phys. Rev. B **98**, 165102 (2018).
  - [78] D. N. Sheng, Y. C. Chen, and Z. Y. Weng, Phase String Effect in a Doped Antiferromagnet, Phys. Rev. Lett. **77**, 5102 (1996).
  - [79] Z. Y. Weng, D. N. Sheng, Y.-C. Chen, and C. S. Ting, Phase string effect in the  $t$ - $J$  model: General theory, Phys. Rev. B **55**, 3894 (1997).
  - [80] K. Shinjo, S. Sota, and T. Tohyama, Effect of phase string on single-hole dynamics in the two-leg Hubbard ladder, Phys. Rev. B **103**, 035141 (2021).
  - [81] S. R. White and D. J. Scalapino, Density Matrix Renormalization Group Study of the Striped Phase in the 2D  $t$ - $J$  Model, Phys. Rev. Lett. **80**, 1272 (1998).
  - [82] S. R. White and D. J. Scalapino, Phase separation and



- stripe formation in the two-dimensional  $t$ - $J$  model: A comparison of numerical results, *Phys. Rev. B* **61**, 6320 (2000).
- [83] S. R. White and D. J. Scalapino, Checkerboard patterns in the  $t$ - $J$  model, *Phys. Rev. B* **70**, 220506(R) (2004).
  - [84] S. R. White and D. J. Scalapino, Pairing on striped  $t$ - $t'$ - $J$  lattices, *Phys. Rev. B* **79**, 220504(R) (2009).
  - [85] P. Corboz, S. R. White, G. Vidal, and M. Troyer, Stripes in the two-dimensional  $t$ - $J$  model with infinite projected entangled-pair states, *Phys. Rev. B* **84**, 041108(R) (2011).
  - [86] W.-J. Hu, F. Becca, and S. Sorella, Absence of static stripes in the two-dimensional  $t$ - $J$  model determined using an accurate and systematic quantum Monte Carlo approach, *Phys. Rev. B* **85**, 081110(R) (2012).
  - [87] P. Corboz, T. M. Rice, and M. Troyer, Competing States in the  $t$ - $J$  Model: Uniform  $d$ -Wave State versus Stripe State, *Phys. Rev. Lett.* **113**, 046402 (2014).
  - [88] B.-X. Zheng, C.-M. Chung, P. Corboz, G. Ehlers, M.-P. Qin, R. M. Noack, H. Shi, S. R. White, S. Zhang, and G. K.-L. Chan, Stripe order in the underdoped region of the two-dimensional Hubbard model, *Science* **358**, 1115 (2017).
  - [89] T. Tohyama, M. Mori, and S. Sota, Dynamical density matrix renormalization group study of spin and charge excitations in the four-leg  $t$ - $t'$ - $J$  ladder, *Phys. Rev. B* **97**, 235137 (2018).
  - [90] H.-C. Jiang and T. P. Devereaux, Superconductivity in the doped Hubbard model and its interplay with next-nearest hopping  $t'$ , *Science* **365**, 1424 (2019).
  - [91] S.-J. Dong, C. Wang, Y.-J. Han, C. Yang and L. He, Stable diagonal stripes in the  $t$ - $J$  model at  $\bar{n}_h = 1/8$  doping from fPEPS calculations, *npj Quantum Mater.* **5**, 28 (2020).
  - [92] T. Tohyama, S. Sota, and S. Yunoki, Spin dynamics in the  $t$ - $t'$ - $J$  model: Dynamical density-matrix renormalization group study, *J. Phys. Soc. Jpn.* **89**, 124709 (2020).
  - [93] V. Marino, F. Becca, and L. F. Tocchio, Stripes in the extended  $t$ - $t'$  Hubbard model: A variational Monte Carlo analysis, *SciPost Phys.* **12**, 180 (2022).
  - [94] D. Xiao, M.-C. Chang, and Q. Niu, Berry phase effects on electronic properties, *Rev. Mod. Phys.* **82**, 1959 (2010).
  - [95] J. Sinova, S. O. Valenzuela, J. Wunderlich, C. H. Back, and T. Jungwirth, Spin Hall effects, *Rev. Mod. Phys.* **87**, 1213 (2015).